Accepted Manuscript

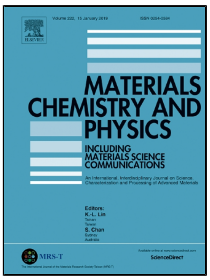

Microstructure–mechanical properties correlation in spark plasma sintered Ti–4.8 wt.% TiB_2 composites

Abbas Sabahi Namini, Amir Motallebzadeh, Behzad Nayebi, Mehdi Shahedi Asl, Maziyar Azadbeh

PII:	S0254-0584(18)31015-0
DOI:	10.1016/j.matchemphys.2018.11.057
Reference:	MAC 21141
To appear in:	*Materials Chemistry and Physics*
Received Date:	17 March 2018
Accepted Date:	26 November 2018

Please cite this article as: Abbas Sabahi Namini, Amir Motallebzadeh, Behzad Nayebi, Mehdi Shahedi Asl, Maziyar Azadbeh, Microstructure–mechanical properties correlation in spark plasma sintered Ti–4.8 wt.% TiB_2 composites, *Materials Chemistry and Physics* (2018), doi: 10.1016/j.matchemphys.2018.11.057

Microstructure–mechanical properties correlation in spark plasma sintered Ti–4.8 wt.% TiB_2 composites

Abbas Sabahi Namini [a,b*], Amir Motallebzadeh [c], Behzad Nayebi [d*] Mehdi Shahedi Asl [d], Maziyar Azadbeh [e]

[a] *Department of Advanced Technologies, University of Mohaghegh Ardabili, Namin, Iran.*

[b] *Department of Engineering Sciences, Sabalan University of Advanced Technologies (SUAT), Namin, Iran.*

[c] *Koc University Surface Science and Technology Center, Istanbul, Turkey*

[d] *Department of Mechanical Engineering, University of Mohaghegh Ardabili, Ardabil, Iran*

[e] *Department of Materials Engineering, Sahand University of Technology, Tabriz, Iran*

**Corresponding Authors:*
Behzad Nayebi (behzad.nayebi@aut.ac.ir)
A. Sabahi Namini (a_sabahi@sut.ac.ir)

Abstract

Ti-TiB_2 composites were fabricated from powder mixtures via spark plasma sintering method. Mechanical behavior of the sintered composites were then investigated via both routine and nanoindentation methods. Results indicated a significant increase in ultimate tensile strength and hardness of the composite, when the sintering temperature is raised. Besides common increase in the relative density of the composite, such a behavior was also attributed to the higher amounts of in-situ formed TiB whiskers. The remarkable reduction in bending strength is probably due to limited formability of unreacted coarse TiB_2 particles and agglomerated in-situ formed phases.

Such findings were then discussed in detail, based on the nanomechanical behavior of the primary and in-situ formed phases in Ti-TiB_2 composite sintered at 1200°C. It was concluded that the superiority of mechanical properties in the mentioned sample may be due to high strength primary and in-situ formed reinforcements distributed homogenously in the matrix. Such reinforcement also provided high strength interfaces, according to interfacial nanoindentation approaches.

Keywords: Spark Plasma Sintering; Titanium matrix composites; Titanium diboride; Mechanical properties; Nanoindentation.

1. Introduction

Besides its unique combination of properties, wear resistance and high-temperature properties of titanium challenge its industrial applications, particularly in aerospace industries. Therefore, several research works have recently focused on improving the

properties of titanium, based on composite-making approach. It has been shown that using reinforcements such as TiN, TiB_2, TiC, B_4C, SiC, etc. can lead to improved wear properties and stiffness of Ti-based alloys, as well as high-temperature strength. Hence, titanium matrix composites (TMCs) reinforced with hard and high-temperature ceramic particles are introduced as promising materials for high-tech and industrial components. Such potential applications are known as the driving force of extensive research works in recent decades [1-12]. Although TMCs are currently used in defense, automobile, aerospace and biomedical applications, there appears to be a great necessity for further research. Particularly, there is a growing tendency in developing the low-cost and repeatable processing methods of TMCs in order to obtain the best combination of achievable properties.

Among several manufacturing methods, In-situ techniques have been developed recently in which, reinforcement phases are directly synthesized during the fabrication process, mainly through chemical reactions between the initial constituents of the composite [9-18]. Although such techniques provide relatively low-cost products, but they deal with some shortcomings, e.g. inhomogeneity of microstructure and the distribution of reinforcements. However, manufacturing methods based on powder metallurgy may overcome such limitation, especially if they include reactive sintering (which can positively be influenced through in-situ formation of secondary and interfacial phases).

Mechanical properties of matrix, reinforcement phases and the matrix/reinforcement interfaces are known as the main influencing factors on the overall mechanical properties of the composite materials. In addition, macroscopic mechanical properties of TMCs are strongly conditioned by the mechanical behavior of possible phases formed from the interactions between the constituents and characteristics of matrix/reinforcement interfaces. So it is necessary to determine the properties of different phases individually and evaluate the interfacial mechanical behavior in heterogeneous regions, particularly, as the mechanical properties of an individual phase in a composite structure may be different with those of its bulk. Therefore, evaluation of mechanical properties of different phases may result in better understanding of the behavior of the composites and consequently lead to improved design of materials.

Whereas micro/macro mechanical evaluations of composite materials are commonly carried out, recently developed techniques such as nano-indentation have provided the possibility of precise understanding of the mechanical behavior of different phases in TMCs, even in nano-scale [13-19]. In this study, the mentioned technique was used to evaluate and measure the mechanical properties of the spark plasma sintered TiB_2 reinforced TMC, containing 4.8 wt.% titanium diboride sintered at 1050 °C. Such a composition has been chosen to clarify densification behavior and strengthening mechanisms of the composite, as it is indicated that TiB_2 content of about 4.8-5 wt.% results in the best combination of properties (maximum tensile strength accompanied with optimum densification behavior) [13] among SPSed Ti-Based composites containing <10 wt.% Mo. Hence, the influences of different SPS temperatures on nano and macro (bulk) mechanical properties of such a composite were investigated to achieve the optimum process parameters for Ti- 4.8 wt.% TiB_2 composites.

2. Experimental procedures

2.1. Materials and processing

Hydride–dehydride Ti (HDH-Ti) powder (particle size <70μm, purity> 98%) and TiB_2 (particle size <50μm, purity> 98%) were used as starting materials. As-received materials were then mixed in turbula mixer (60 rpm) for 5 hours. Finally, a powder mixture containing 95.2 wt. % Ti and 4.8 wt. % TiB_2 was obtained. Five samples were then prepared and spark plasma sintered at different temperatures (750-1350°C) for 5 minutes under a pressure of 50 MPa. Samples were then coded based on the sintering temperatures, according to coding system presented in Table. 1. The heating schedule and applied pressure of the sintering process are graphically presented in Fig. 1.

Table. 1. Codding system of the prepared samples based on their sintering temperatures.

Code	T750	T900	T1050	T1200	T1350
Sintering Temperature (°C)	750	900	1050	1200	1350

2.2. Physical and mechanical properties tests

The apparent and theoretical densities of the sintered composites were measured based on Archimedes principle and rule of mixtures, respectively. The obtained values were then

used to calculate the relative density of the samples. Macro/micro-hardness values of the samples were measured via Vickers indenter (ESEWAY, UK) on the polished surface of the samples, using 30 kg and 300 g applied load, respectively. The values of hardness were concluded as the mean of at least six indentation runs. The plates were then precisely cut via electrical discharge machine (EDM) in order to provide standard samples for mechanical properties test. Three-point bending strength, room and high temperature tensile strength tests were carried out using a universal testing machine (STM-250-equipped with a resistance furnace). The dimensions of the cut samples for the bending tests were 3 × 4 × 34 (mm) with a span of 15 mm. Three tests were performed to get an average value of bending strength and to check the reliability of the results. The reported flexural strength values have been calculated based on Eq. 1 [14]:

$$\sigma_b = \frac{1.5FL}{bd^2} \qquad (1)$$

where σ_b is flexural strength (MPa), F shows the load at a given point on the load deflection curve (N), L is support span, (mm), b is the width of the test beam in mm and d represents the thickness of the tested sample (mm). The dimensions of room and high temperature (600°C) tensile specimens were 2 × 5 × 15 (mm) and 18 × 2 × 6 (mm), respectively. Each test was repeated at least four times and the average values were reported.

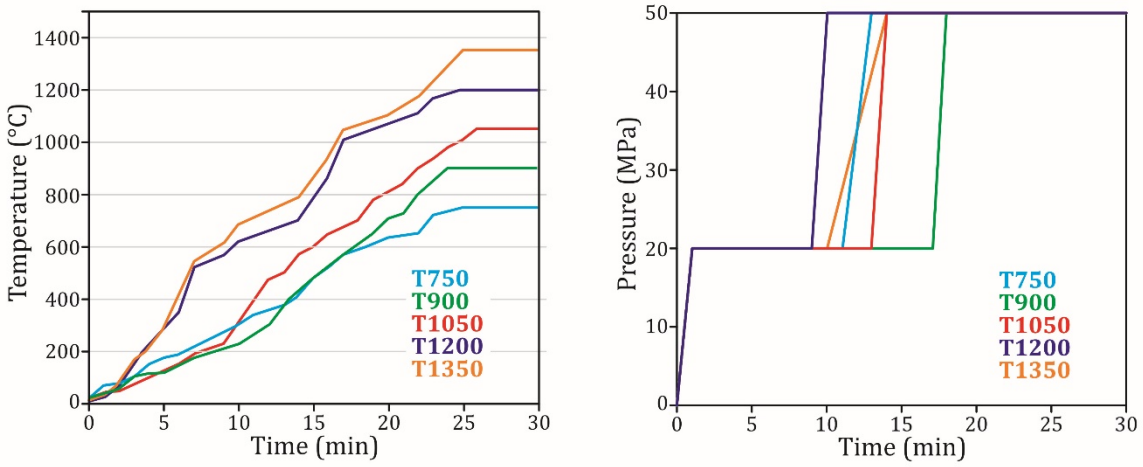

(a) (b)

Fig. 1. (a) Heating and (b) pressing schedule of the samples through SPS process.

2.3. Nanoindentation

Depth sensing nano-indentation test equipment (Agilent G200, USA) with Berkovich diamond indenter tip was used to make ultra-low load (5 – 150 mN) indentations in selected locations and investigate the mechanical properties of constituent phases in T1200 sample. The displacement of the indenter was continuously recorded to obtain nano-hardness, elastic modulus and contact stiffness of titanium matrix and reinforcements, based on Oliver-Pharr method [19-33]. Indentation zones were precisely selected on matrix and reinforcement phases as well as matrix/reinforcement interfaces, which cannot be evaluated via other testing methods. The mechanical properties of the mentioned regions and phases were calculated by averaging the obtained values from six indentations for each region. Adequate indentation distances were considered to minimize the overlap effect.

The maximum applied load was 100 mN for all indents. Calculations were carried out based on the general concepts of each property. Using the Berkovich indenter, hardness was calculated based on Eq. 2 [19-33]:

$$H = \frac{P_{Max}}{A_C} \qquad (2)$$

In which, H represents hardness, P_{Max} is allotted to the maximum applied load and A_C shows the projected area of indentation and can be calculated as follows:

$$A_C = 24.5 \times h_C^{\,2} \qquad (3)$$

Where h_C is the contact depth at the maximum load. It is indicated that the actual depth of contact (h_C) is normally less than the total depth of indenter penetration [24]. Therefore a corrected depth of contact should be used, which is calculated as follows [19-33]:

$$h_C = h_{Max} - \alpha \frac{P_{Max}}{S} \qquad (4)$$

Where h_{Max} is the indenter displacement measured at maximum load, α is a geometrical constant related to the shape of the indenter (α=0.75 for Berkovich tips), and S is the contact stiffness. Based on Oliver-Pharr method, contact stiffness can be calculated using the slope of unloading curve at maximum load (P_{max}), as follows [19-33]:

$$S = \left(\frac{dP}{dh}\right)_{h=hMax} = \delta \frac{2}{\sqrt{\pi}} E_m \sqrt{A_C} \qquad (5)$$

In which, δ, an indenter geometry-depended constant equals to 1.034 in here (Berkovich indenter). Modified elastic modulus, E_m, represents the elastic modulus that considers the elastic contributions of specimen and the indenter tip, and calculated using Eq. 6 [19-33]:

$$\frac{1}{E_m} = \frac{1-\nu^2_s}{E_s} + \frac{1-\nu^2_i}{E_i} \quad (6)$$

Here, E_i and E_s are the relevant elastic modulus of the indenter and sample, whereas υ_i and υ_s are the Poisson's ratio of the indenter and the specimen, respectively.

3. Results and discussion

3.1. Relative density

Fig. 2 presents the effect of sintering temperature on the relative density of the sintered composites. The plot shows that the relative density of the sintered composites directly changes with the sintering temperature, which means that the higher sintering temperature promotes higher rates of porosity removal and consequently, improved densification. As it can be clearly seen in Fig. 2, increasing the sintering temperature from 750 to 1200 °C leads to relative density enhancement from 93.90 to 99.88 %. It should be noted that the highest slope of the relative density vs. sintering temperature curve is observed between 750 to 900 °C, which may be due to the activation of more diffusion mechanism, e.g. bulk diffusion. Formation of TiB whiskers may also considered as another effective factor in porosity removal and densification. Therefore, it can be concluded that with increasing the sintering temperature from 750 to 900℃, the relative density of the sintered composite enhances from 93.90 % to 98.46 % which is reasonably due to the higher diffusion and the formation of TiB whickers in vacant positions between the particles. Such a collaboration also results in near-fully dense Ti-TiB composite at 1200 °C (due to increased temperature and diffusion rate). However, a slight decrease in the relative density of T1350 sample can be attributed to the grain growth surpassing densification, which postpones the porosity removal. Optical microscopy images presented in Fig. 3 indicate the excessive grain growth of T1350 sample in comparison with T1200 sample.

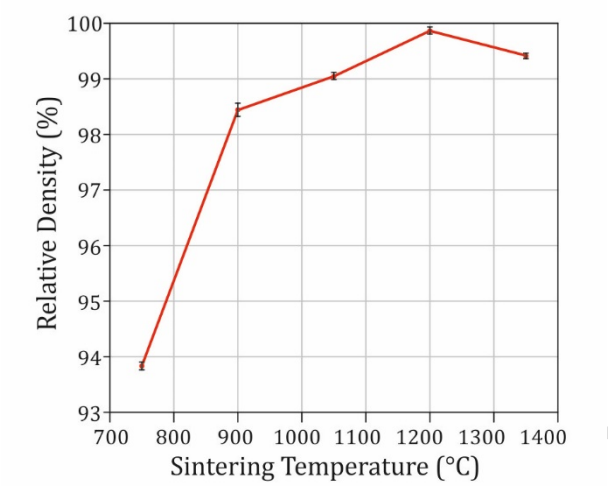

Fig. 2. Relative density of the samples vs. the sintering temperature.

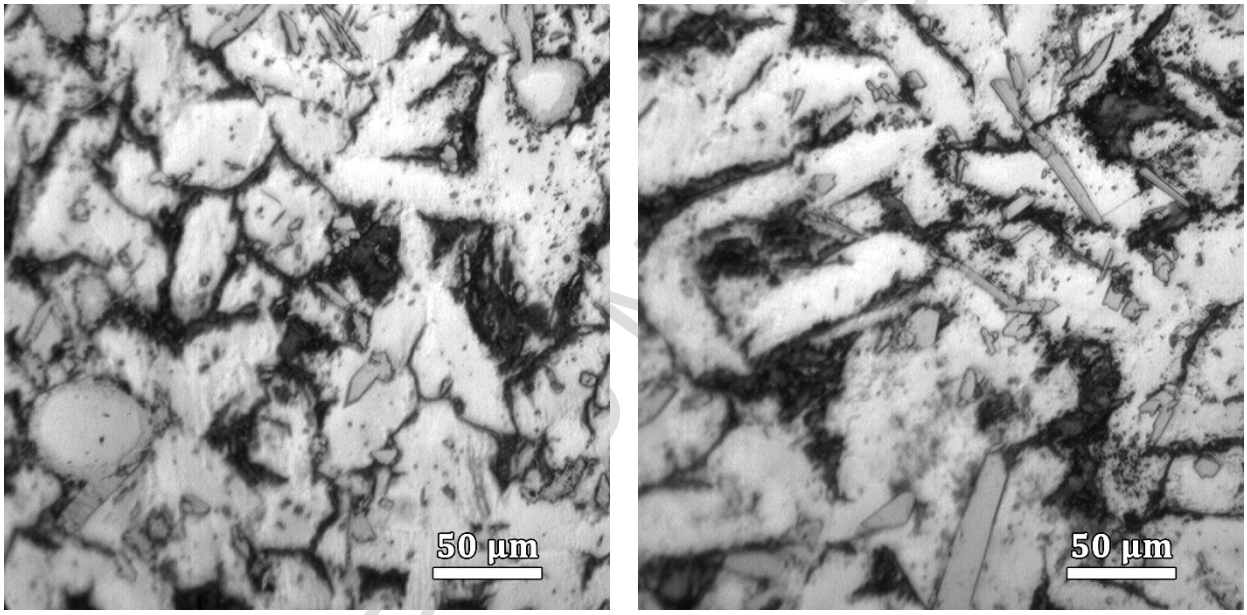

(a) (b)

Fig. 3. Optical microscopy images of the microstructure of (a) T1200 and (b) T1350 samples, indicate the excessive grain growth in sample sintered at 1350°C.

As the sintering in practice is the control of both densification and grain growth and many other physical and mechanical properties, and it benefits from both a high relative density and a small grain size, achieving the optimum sintering temperature is of great importance. According to the obtained results, by rising the sintering temperature, the porosity percentage of the sintered compacts decreases and near fully dense composites were obtained by SPS at temperatures higher than 1050 °C. Besides, the increase in porosity

percentage of T1350 compared to T1200, can be attributed to few pores generated in the microstructure due to the growth of matrix grains. Microstructural observations obviously (not shown here) indicated that the samples fabricated at 750 and 900 °C have a non-dense microstructure and some large pores. When the sintering temperature increases to 1050 °C, it can be seen that the macroscopic pores are disappeared and a more compact microstructure is obtained with less than one percent porosity. It is a fact that grain growth kinetics is governed by grain boundary mobility, and one of the factors responsible for grain boundary mobility is the temperature. On the other hand, the short sintering time (in SPS method) decreases the major drawback potential induced by the high-temperature process, which is the grain growth tendency with temperature and time in the sintered material. However, in this study as the sintering temperature exceeds 1200 °C, the applied high temperature softens the titanium matrix, the growth inhibiting effect seems to be faded, alpha and beta layers grow together and the size of in-situ formed TiB whiskers increases, which have a negative impact on the mechanical properties.

Clarifying the abovementioned discussions, it should be added that during the solid state sintering processes, the reduction in total interfacial energy as the driving force for progression of sintering occurs through both densification and grain growth, which are competing phenomena. The porosity removal at higher sintering temperatures, which leads to the extreme grain growth, is difficult because the size of the pores entrapped between the grains becomes larger. As the progression of densification (increasing the relative density) depends on the elimination of porosity, the growth of grains prevents the material to be easily densified.

3.2. Mechanical properties

3.2.1. Hardness

Fig. 4 presents the variation of macro/micro-hardness vs. sintering temperature for the Ti-4.8TiB_2 composites. As it can be clearly seen, T750 sample exhibits the lowest micro-hardness value (213 HV0.3), whereas the highest value was observed in T1350 (541 HV0.3). On one hand, such a variation may be due to lower densities of samples sintered at lower temperatures. On the other hand, the size and the volume fraction of the synthesized TiB whiskers can be considered as effective factor. In the latter case, it should be clarified

that the smaller the size and the volume fraction of TiB whiskers, the lower the possibility of contact with the indenter. Hence, lower micro-hardness values may be obtained in samples SPSed at lower temperatures. According to the reported macro-hardness (the average of six indentations obtained from different locations), it is shown that the value increases by nearly 140 % (from 178 HV30 for T750 to 428 HV30) as the sintering temperature enhances to 1200°C. Increment of hardness as a function of sintering temperature is attributed to increase in relative density and the generation of more volume fraction of TiB whiskers compared to parent TiB_2 particles. The optical and scanning electron micrographs of the processed composite sintered at 1200°C are presented in Fig. 5, which show the unreacted TiB_2 particles and the in-situ formed TiB whiskers. The reaction mechanisms of spark plasma sintered Ti–TiB_w composite was discussed in previous work [13], in which the investigations were mainly focused on the effects of the volume fraction of TiB_2 reinforcement on microstructural and mechanical properties of titanium matrix composites sintered at 1050°C. The difference in the macro-hardness and the micro-hardness is often ascribed to the size effect (i.e., the hardness reduces with increase in load). According to the research conducted in many studies, it has been determined that the macro-hardness of almost any material is lower than its micro-hardness, since the load applied in Vicker's micro-hardness is usually lower than that applied in macro-hardness [34-35]. Fig. 4 also indicates that the difference between macro-hardness and micro-hardness increases with rising sintering temperature.

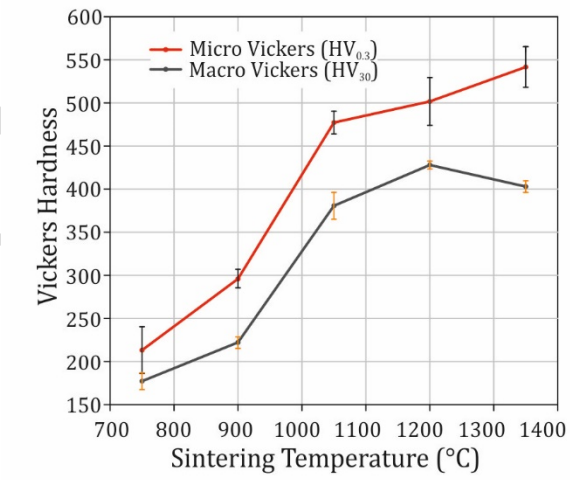

Fig. 4. The macro/micro hardness variation vs. the SPS temperature.

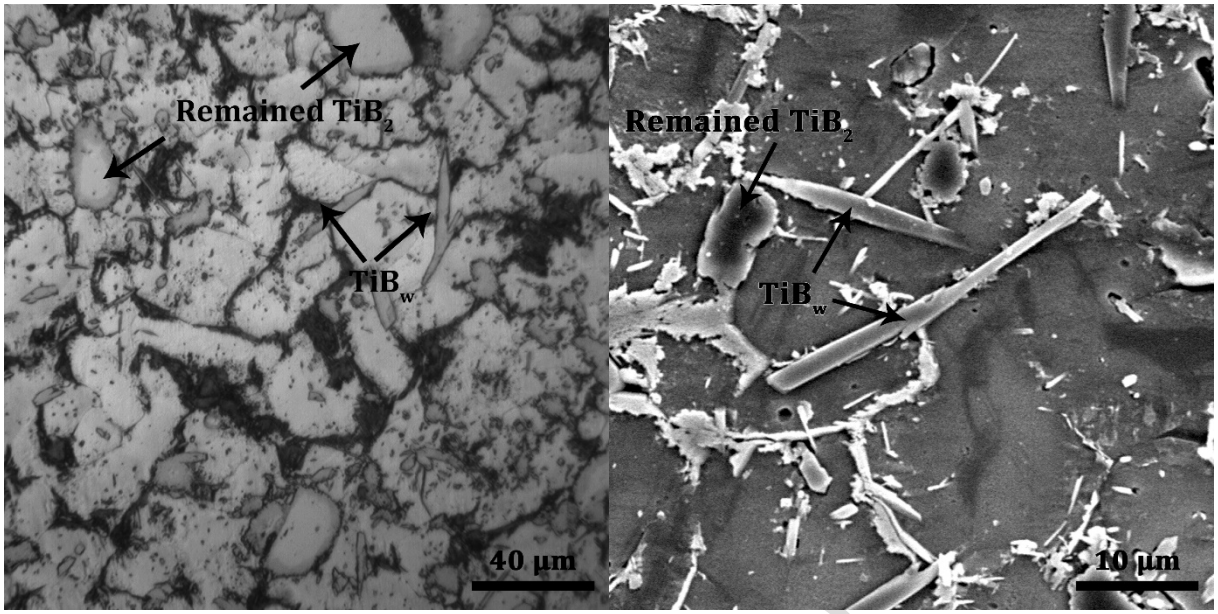

(a) (b)

Fig. 5. (a) Optical and (b) SEM images of the polished surface of sample sintered at 1200°C

3.2.2. Flexural strength

Fig. 6 represents the effects of SPS temperature on bending strength of Ti-TiB_2 composites. The variation trend of such a plot can be illustrated if the amount of in-situ formed TiB whiskers and relative density changes are considered into account. According to the obtained results, increasing the sintering temperature from 750 to 1050°C resulted in rising the relative density and subsequently, increasing the bending strength from 805 MPa to 1273 MPa (or by 58 %). However, as the sintering temperature exceeds 1050°C, the volume fraction and size of the TiB whiskers grow and then, cause a drop in bending strength. Such a decreasing trend can be attributed to the plastic restraint applied by TiB whiskers on the matrix. TiB whisker tips on both sides can act as stress concentration sites, which intensify the plastic flow of the matrix in comparison with equiaxed TiB_2 particles. Therefore, higher amounts of TiB whiskers can affect the bending strength of the composite, negatively. Anyway, it can be concluded that in sintering temperature range of 750 to 1050°C, the dominant factor was porosity reduction, which resulted in increasing flexural strength from 805 to 1273 MPa. When the sintering temperature raised from 1050 to 1350°C, the fraction of TiB whiskers manifested as the key factor and caused decreasing flexural strength of the composite from 1273 to 967 MPa.

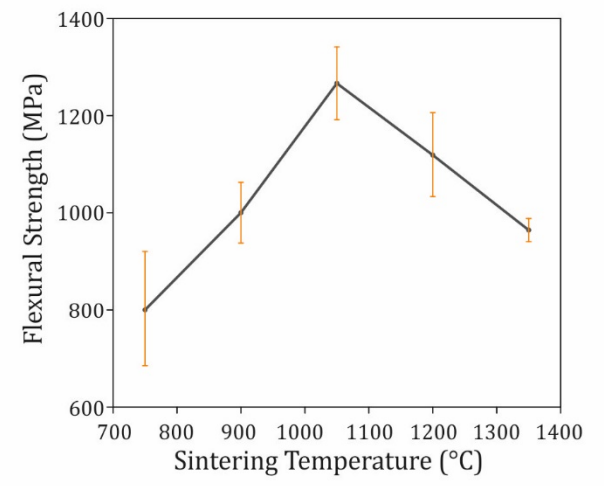

Fig. 6. Influence of sintering temperature on flexural strength of Ti-4.8 wt.% TiB_2 composites.

3.2.3. Tensile strength

The results of the room temperature tensile test of the sintered composites are shown in Fig. 7. Improved tensile strength was obviously achieved when the sintering temperature increased. As it can be clearly seen, T750 sample exhibits the lowest UTS among the samples, which logically can be attributed to its lowest density and highest fraction of porosity. Fig. 7 indicates that the ultimate tensile strength of the samples is following an overall incremental trend, when the sintering temperature is raised from 900 to 1200°C. Nevertheless, whereas the maximum UTS (541 MPa) was achieved for T1200, a slight decrease was observed for T1350 sample which experienced the highest sintering temperature. Such a UTS drop, as previously discussed about bending strength, may be due to the higher volume fraction of TiB whiskers which provide increased stress concentration sites.

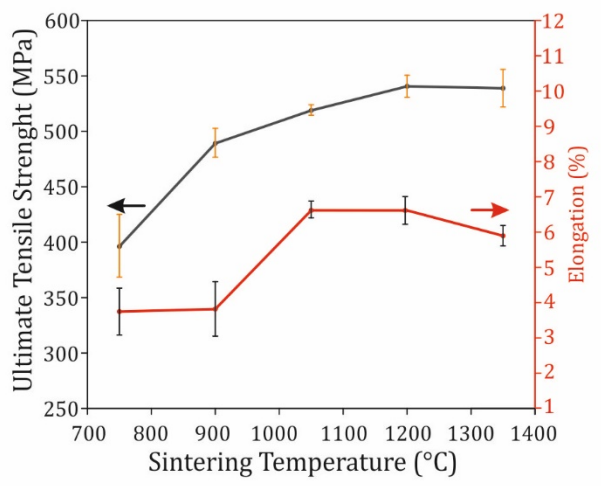

Fig. 7. Room temperature tensile properties of the specimens sintered at different temperatures.

Nevertheless the incremental trend of UTS, ductility reduction was observed for samples T1050 to T1350, which means the improved UTS was achieved scarifying the ductility. Unreacted TiB_2 particles and agglomerated in-situ formed TiB whiskers can be considered responsible of such a ductility drop. Low ductility of titanium matrix can be introduced as another effective factor on the elongation of composites. Strengthening in whisker reinforced composites, generally is believed to be a result of combined effects of geometrically increased density of dislocations (due to stresses induced during cooling process), grain refinement, solid-solution, dislocation/whisker interactions and load/stress transfer across the matrix and whisker reinforcements. Some of these factors may affect the tensile strength of near fully-dense composites investigated in this study.

The tensile stress-strain curves of T1200 and T1350 samples at 600°C (Fig. 8) are selected to discuss the stress-strain behavior of the sintered composites at high temperatures. These results suggest that the tensile strength of the T1200 is higher than that of the sample sintered at 1350°C.

In comparison with the results of room temperature tests, it is also clear that the strengthening effect of in-situ formed TiB whiskers was weakened. Such a shortcoming may be due to the dynamic recovery/recrystallization (DRV/DRX) of the titanium matrix [36], which promotes the movement of dislocation and consequently, the easier plastic deformation of the matrix. In fact, it may interrupt the process of stress transfer from matrix to the reinforcements, and lead to lower mechanical strength.

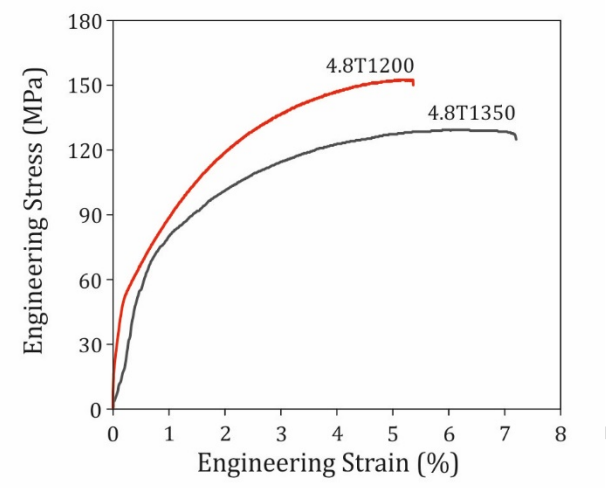

Fig. 8. Engineering tensile stress–strain curves of the T1200 and T1350 composites tested at 600°C.

It is also worth to note that higher temperatures may influence the matrix/reinforcement interface, which plays a key role in mechanical behavior of the composites. The strengthening effect of TiB whiskers and remained TiB_2 particles (reinforcement phases) depends on their interfaces with the titanium matrix. Elevated temperatures may promote atomic diffusion and change the mechanical response as well as the thickness and morphology of the interfaces, which consequently affect the mechanical properties of the bulk composite.

3.2.4. Nanoindentation

Instrumented nano-indentation test was used to measure the mechanical properties of T1200 sample. The technique has several applications in characterization of in-situ formed phases in composites and even recently developed materials e.g. bulk metallic glasses (BGMs) [37-38]. Obtained results including hardness, young's modulus and contact stiffness for different existed phases in the microstructure of T1200 sample are presented in Table. 2.

Table. 2: Calculated mean values of elastic modulus, hardness and contact stiffness for α-Ti, β-Ti, TiB_w, TiB_2-corona and TiB_2 phases in T1200 sample.

	α-Ti	**β-Ti**	**TiB whisker**	**TiB_2 corona**	**TiB_2**
E (GPa)	130.54	111.34	293.97	359.55	459.80
H (GPa)	4.27	4.70	21.30	22.42	38.41
Stiffness (N/mm)	103.80	88.98	106.47	165.21	194.73

According to Table. 2, it appears that the values of nano-hardness follow an incremental trend for α-Ti, β-Ti, TiB_w, TiB_2-corona and TiB_2. Moreover, the elastic modulus and stiffness show the maximum and minimum values for TiB_2 and β-Ti, respectively. SEM micrograph presented in Fig. 9a shows the microstructure of T1200 sample, including a TiB2 particle surrounded with a Boron-rich solid solution corona and some TiB whiskers lied in titanium matrix. Optical micrograph of the indents is also presented in Fig. 9b.

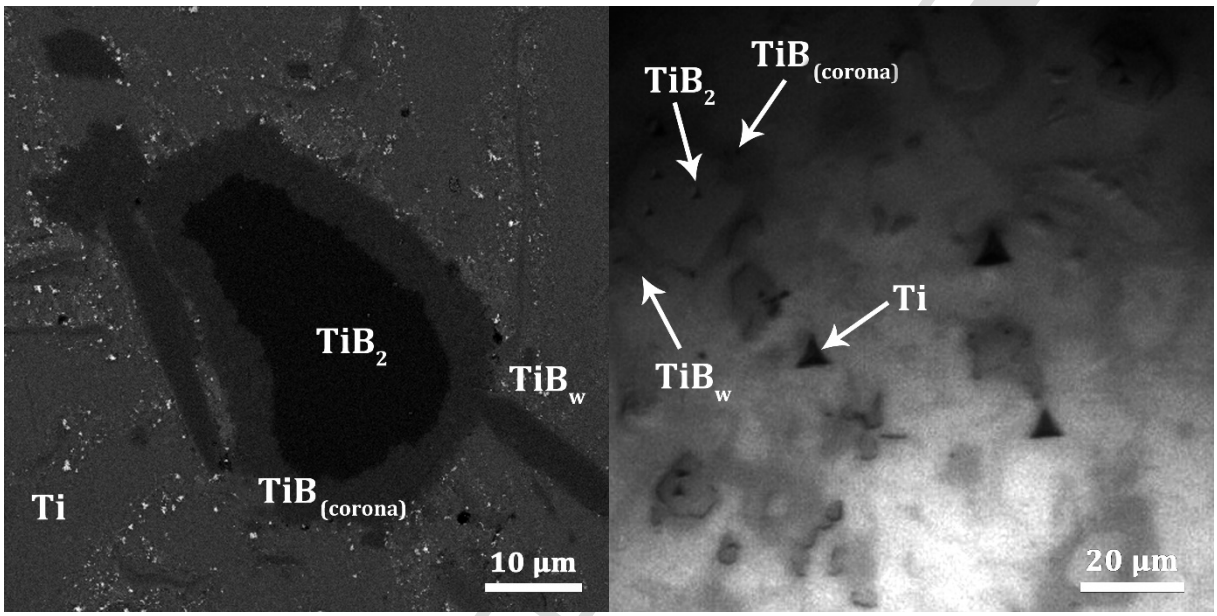

(a) (b)

Fig. 9. (a) SEM micrograph of the microstructure of T1200 sample and (b) Optical micrograph of the residual imprints on the surface of T1200 after indentation by Berkovich diamond nano-indenter tip.

Typical load-contact depth curves for different phases in the composite sintered at 1200 ℃ are shown in Fig. 10a, in which the load required to reach the same penetration depth decreases respectively for TiB_2, TiB_2-corona, TiB_w, β-Ti and α-Ti, which confirms that TiB_2 has the highest hardness and α-Ti has the lowest. Curves of hardness and elastic modulus of TiB_2 corona and TiB_w as a function of contact depth can be divided into three regions as shown in Fig. 10c-d. In fact, the primary rise in hardness seems to be due to the elastic contact between indenter tip and the investigated phase. So, the value of hardness measured under the low applied load of indenter cannot reflect the TiB_2 corona and TiB_w hardness and will be less than the hardness of the mentioned phase. At higher loads, the

influence of the titanium matrix is felt and the hardness decreases according to the relative hardness of the ceramic reinforcement phase and titanium. Finally, obtaining a fully plastic zone, the hardness reaches a plateau. Moreover, no drop was occurred in hardness of TiB_2 and titanium phase (alpha and beta) at large penetration depths, which is probably due to the higher thickness of TiB_2 in comparison with the maximum penetration depth and uniform mechanical properties of titanium, respectively. The variation of elastic modulus with contact depth shows relatively the same trend (Fig. 10c). Also, the increment of stiffness with changes in depth (Fig. 10b) attributes to work hardening made on different phases due to the applied load of indenter. It is remarkable to note that, the contact stiffness values of all phases increased linearly proportional to contact depth, but the contact stiffness value of TiB_w increased with a slightly decreasing slope. According to the investigations performed by Li and Bhushan [22], for a uniform material with a constant elastic modulus value, the contact stiffness is linearly proportional to contact depth, but for a non-uniform material, the stiffness of the examined phase changes when the chemical composition varies at different indentation depth. So it seems that due to the non-uniform structure of TiB_w under the indented region, the increment of stiffness with changes in depth is non-linear.

The nano-mechanical properties of TiB_2-corona, as the interfacial phase, address a strong connection between the matrix and the reinforcement phases of the composite. As it can be clearly seen in Fig. 10, such a phase approximately shows the average mechanical properties of the matrix and reinforcement phases which indicates a stiff connection between the mentioned phase and both of the matrix and reinforcements. The influences of such interface phase, manifest as the superior macro-mechanical properties of T1200 sample in comparison with the others, although adequate fraction of TiB whickers in T1200 sample should also be considered. However, at elevated temperatures, the mechanical properties of the mentioned interfacial phase may decrease due to the extensive atomic diffusion, leading to poor macro-mechanical properties of the composite, as discussed before.

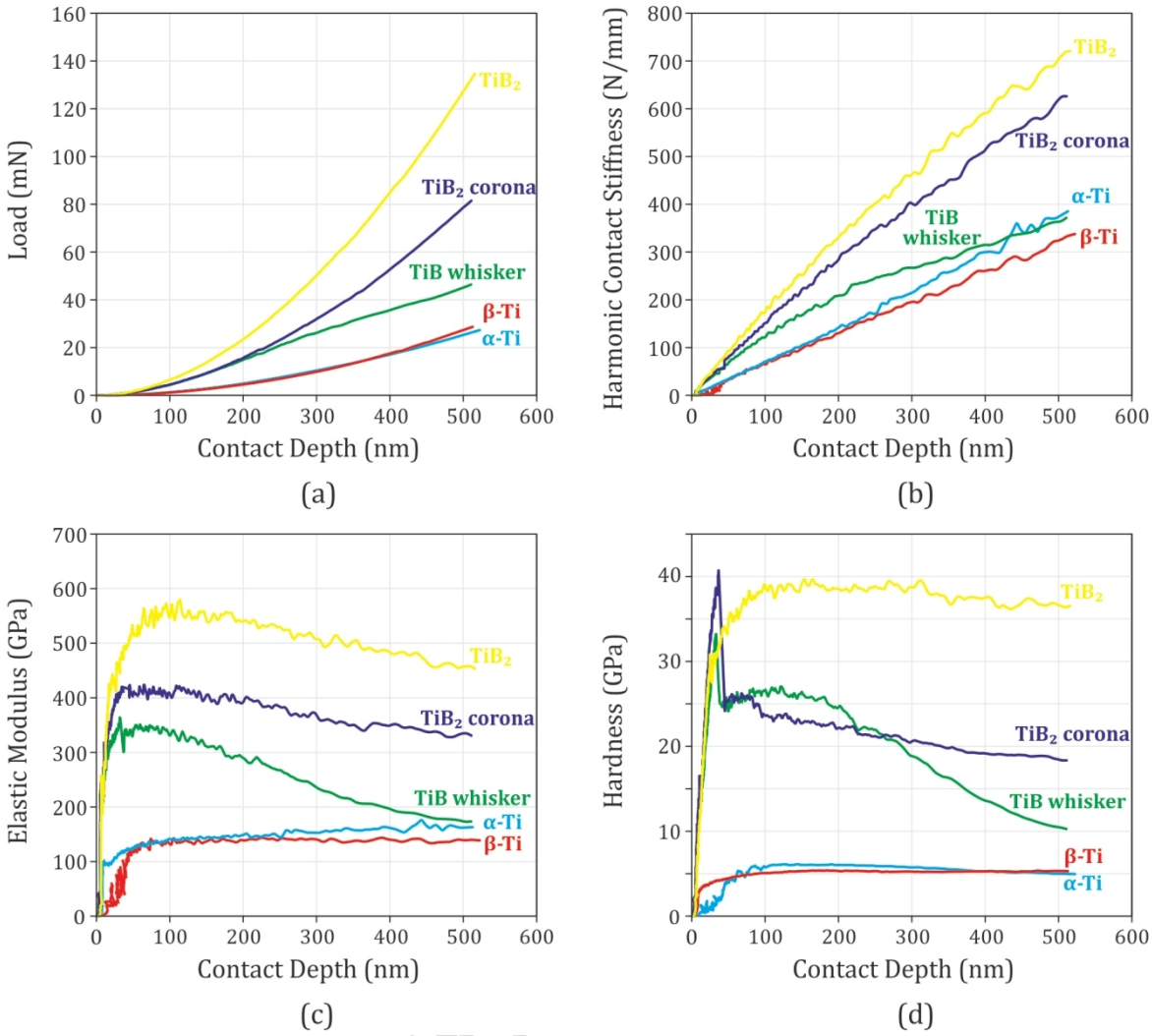

Fig. 10. Obtained nano-indentation curves (a) load, (b) harmonic contact stiffness, (c) elastic modulus and (d) hardness as a function of contact depth for the existed TiB_2, TiB_2-corona, TiB_w, β-Ti and α-Ti phases in T1200 composite.

4. Conclusions

The in-situ synthesized TiB reinforced titanium matrix composites were fabricated using spark plasma sintering method. The effects of sintering temperature on the mechanical properties were investigated using controlled experiments. The results indicated that the Ti-TiB_2 composites sintered at 1200°C show the highest relative density of 99.88% along with a good combination of ultimate tensile strength (541 MPa), elongation (6.62%), macro-hardness (428 HV30) and micro-hardness (501 HV0.3). The increase of above mentioned mechanical properties with rising sintering temperature is mainly attributed to

increased relative density and formation of higher volume fractions of TiB whiskers. While decreasing the bending strength from 1273 to 967 MPa, the sintering temperature raised from 1050 to 1350°C which is possibly due to the plastic limitation imposed on the matrix by the existed agglomerated ceramic phases and stress concentration at the tips of TiB whiskers which impede the plastic flow of the matrix. Besides, compared with room temperature properties, the tensile strength of the composites has a significant decrement at elevated temperature, mainly attributed to the variations in the mechanical properties of the interfacial phase, grain growth and softening of the matrix. Nanoindentational approach was conducted to illustrate the superior mechanical properties of sample sintered at 1200°C, and the elastic modulus, hardness and stiffness of phases existing in Ti-TiB_w composite were also measured. Results indicated that the elastic modulus and stiffness were increased for α-Ti, β-Ti, TiB_w, TiB_2-corona and TiB_2, respectively.

Acknowledgements

The authors would like to express their sincere gratitude to Mr. Alireza Naghizadeh for his helps during microstructural characterizations. Authors also appreciate technical guidelines and helps of Dr. Mojtaba Yazdani and his colleagues at Materials Research Laboratory (MRLab) of Sahand University of Technology.

References

[1] B. S. Li, J. L. Shang, J. J. Guo, H. Z. Fu, Formation of TiB_w reinforcement in in-situ titanium matrix composites, Materials Science, 39 (2004) 1131 – 1133.

[2] B.S. Li, J.L. Shang, J.J. Guo, H.Z. Fu, In situ observation of fracture behavior of in situ TiB_w/Ti composites, Materials Science and Engineering A, 383 (2004) 316–322.

[3] L.J. Huanga, L. Genga, H.X. Peng, In situ (TiBw + TiCp)/Ti6Al4V composites with a network reinforcement distribution, Materials Science and Engineering A 527 (2010) 6723–6727.

[4] Z. Yan, F. Chen, Y. Cai, Y. Zheng, Microstructure and mechanical properties of in-situ synthesized TiB whiskers reinforced titanium matrix composites by high-velocity compaction, Powder Technology 267 (2014) 309–314.

[5] A. Sabahi Namini, M. Azadbeh, M. Shahedi Asl, Effects of in-situ formed TiB whiskers on microstructure and mechanical properties of spark plasma sintered Ti–B_4C and Ti–TiB_2 composites, Scientia Iranica 24 [3] (2017).

[6] L. J. Huang a, L. Geng, H.X. Peng, K. Balasubramaniam, G.S. Wang, Effects of sintering parameters on the microstructure and tensile properties of in situ TiBw/Ti6Al4V composites with a novel network architecture, Materials and Design 32 (2011) 3347–3353.

[7] M. Y. Koo, J. S. Park, M. K. Park, K. T. Kim, S. H. Hong, Effect of aspect ratios of in situ formed TiB whiskers on the mechanical properties of TiBw/Ti–6Al–4V composites, Scripta Materialia 66 (2012) 487–490.

[8] A. Sabahi Namini, S.N. Seyed Gogani, M. Shahedi Asl, K. Farhadi, M. Ghassemi Kakroudi, A. Mohammadzadeh, Microstructural development and mechanical properties of hot pressed SiC reinforced TiB_2 based composite, Int. J. Refract. Metal. Hard Mater. 51 (2015) 169–179.

[9] V.S. Balaji, S. Kumaran, Densification and microstructural studies of titanium–boron carbide (B_4C) powder mixture during spark plasma sintering, Powder Technology 264 (2014) 536–540.

[10] C. Zhang, F. Kong, S. Xiao, H. Niu, L. Xu, Y. Chen, Evolution of microstructural characteristic and tensile properties during preparation of TiB/Ti composite sheet, Materials and Design 36 (2012) 505–510.

[11] P. Nandwana, J.Y. Hwang, M.Y. Koo, J. Tiley, S.H. Hong, R. Banerjee, Formation of equiaxed alpha and titanium nitride precipitates in spark plasma sintered TiB/Ti–6Al–4V composites, Materials Letters 83 (2012) 202–205.

[12] C.J. Zhang, F.T. Kong, S.L. Xiao, E.T. Zhao, L.J. Xu, Y.Y. Chen, Evolution of microstructure and tensile properties of in situ titanium matrix composites with volume fraction of (TiB + TiC) reinforcements, Materials Science and Engineering A 548 (2012) 152– 160.

[13] A. Sabahi Namini, M. Azadbeh, M. Shahedi Asl, Effect of TiB_2 content on the characteristics of spark plasma sintered Ti–TiB_w composites, Advanced Powder Technology, 28, (2017) 1564–1572.

[14] H. Feng, D. Jia, Y. Zhou, Spark plasma sintering reaction synthesized TiB reinforced titanium matrix composites, Composites: Part A 36 (2005) 558–563.

[15] A. Sabahi Namini, M. Azadbeh, Microstructural characterisation and mechanical properties of spark plasma-sintered TiB_2-reinforced titanium matrix composite, J. Powder Metall. 60 (2017) 22–32.

[16] S. Ghesmati Tabrizi, S. Abdolkarim Sajjadi, A. Babakhani, W. Lu, Influence of spark plasma sintering and subsequent hot rolling on microstructure and flexural behavior of in-

situ TiB and TiC reinforced Ti6Al4Vcomposite, Materials Science and Engineering A 624 (2015) 271–278.
[17] H. Feng, Y. Zhou, D. Jia, Q. Meng, Microstructure and mechanical properties of in situ TiB reinforced titanium matrix composites based on Ti–FeMo–B prepared by spark plasma sintering, Composites Science and Technology 64 (2004) 2495–2500.

[18] S. Gorsse, Y. Le Petitcorps, S. Matar, F. Rebillat, Investigation of the Young's modulus of TiB needles in situ produced in titanium matrix composite, Materials Science and Engineering A340 (2003) 80-87.

[19] V. Kralik, J. Nemecek, Comparison of nanoindentation techniques for local mechanical quantification of aluminium alloy, Materials Science and Engineering A 618 (2014) 118–128.

[20] A.C. Fischer-Cripps, Critical review of analysis and interpretation of nanoindentation test data, Surface and Coatings Technology 200 (2006) 4153 – 4165.

[21] P. Majumdar, S.B. Singh, M. Chakraborty, Elastic modulus of biomedical titanium alloys by nano-indentation and ultrasonic techniques—A comparative study, Materials Science and Engineering A 489 (2008) 419–425.

[22] X. Li, B. Bhushan, A review of nanoindentation continuous stiffness measurement technique and its applications, Materials Characterization 48 (2002) 11 – 36.

[23] M. Selvakumar, P. Chandrasekar, B. Ravisankar, J. N. Balaraju, and M. Mohanraj, Mechanical properties of titanium-titanium boride composites through nanoindentation and ultrasonic technique – An evaluation perspective, Powder Metallurgy and Metal Ceramics 53 (2015) 9-10.

[24] W.C. Oliver, G.M. Pharr, Measurement of hardness and elastic modulus by instrumented indentation: Advances in understanding and refinements to methodology J. Mater. Res. 19 (2004).

[25] G. Cao, L. Geng, Elastic Properties of Titanium Monoboride Measured by Nanoindentation, Journal of American Ceramic Society 89 [12] (2006) 3836–3838.

[26] K. Morsi, V. V. Patel, K. S. Moon, J. E. Garay, Current-activated pressure-assisted sintering (CAPAS) and nanoindentation mapping of dual matrix composites, Journal of Material Science 43 (2008) 4050–4056.

[27] S. Mania, C. Palanisamy, M. Murugesan, R. Balasubramanian, Estimation of distinctive mechanical properties of spark plasma sintered titanium–titanium boride composites through nano-indentation technique, International Journal of Material Research 106 (2015) 11.

[28] A.F. Gerday, M. Ben Bettaieb, L. Duchêne, N. Clement, H. Diarra, A.M. Habraken, Material behavior of the hexagonal alpha phase of a titanium alloy identified from nanoindentation tests, European Journal of Mechanics A/Solids 30 (2011) 248-255.

[29] A. Urena, J. Rams, M.D. Escalera, M. Sanchez, Characterization of interfacial mechanical properties in carbon fiber/aluminium matrix composites by the nanoindentation technique, Composites Science and Technology 65 (2005) 2025–2038.

[30] F.K. Mante, G.R. Baran, B. Lucas, Nanoindentation studies of titanium single crystals Biomaterials 20 (1999) 1051-1055.

[31] K. M. Mussert, W. P. Vellinga, A. Bakker, S. V. Zwaag, A nano-indentation study on the mechanical behaviour of the matrix material in an AA6061 - Al_2O_3 MMC, Journal of Materials Science 37 (2002) 789– 794.

[32] J. Kwon, M.C. Brandes, P. S. Phani, A.P. Pilchak, Y.F. Gao, E.P. George, G.M. Pharr, M.J. Mills, Characterization of deformation anisotropies in an a-Ti alloy by nanoindentation and electron microscopy, Acta Materialia 61 (2013) 4743–4756.

[33] Z.H. Melgarejo, P.J. Resto, D.S. Stone, O.M. Suarez, Study of particle–matrix interaction in Al/AlB_2 composite via nanoindentation, Materials Characterization 61 (2012) 135-140.

[34] Y. Prawoto, Design, stress analysis and metallurgy of automotive coil and leaf springs: fundamental principles and applications, Morrisville, NC: Lulu Enterprise Inc., 2017.

[35] Y. Prawoto, Integration of mechanics into materials science research: a guide for material researchers in analytical, computational and experimental methods, Morrisville, NC: Lulu Enterprise Inc., 2013.

[36] M. J. Tan, X. J. Zhu, Dynamic recrystallization in commercially pure titanium, Journal of achievements in materials and manufacturing engineering 18, Issue 1-2, 2006.

[37] A. Ayyagari, T. W. Scharf, S. Mukherjee, Dry reciprocating sliding wear behavior and mechanisms of bulk metallic glass composites, Wear 350–351 (2016) 56-62.

[38] A. Ayyagari, V. Hasannaeimi, H. Arora, S. Mukherjee, Electrochemical and friction characteristics of metallic glass composites at the microstructural length-scales, Scientific Reports 17; 8(1): 906 (2018) doi: 10.1038/s41598-018-19488-7.

Captions of Tables:

Table. 1. Codding system of the prepared samples based on their sintering temperatures.

Table. 2: Calculated mean values of elastic modulus, hardness and contact stiffness for α-Ti, β-Ti, TiB_w, TiB_2-corona and TiB_2 phases in T1200 sample.

Figure captions:

Fig. 1. (a) Heating and (b) pressing schedule of the samples through SPS process.

Fig. 2. Relative density of the samples vs. the sintering temperature.

Fig. 3. Optical microscopy images of the microstructure of (a) T1200 and (b) T1350 samples, indicate the excessive grain growth in sample sintered at 1350°C.

Fig. 4. The macro/micro hardness variation vs. the SPS temperature.

Fig. 5. (a) Optical and (b) SEM images of the polished surface of sample sintered at 1200°C

Fig. 6. Influence of sintering temperature on flexural strength of Ti-4.8 wt.% TiB_2 composites.

Fig. 7. Room temperature tensile properties of the specimens sintered at different temperatures.

Fig. 8. Engineering tensile stress–strain curves of the T1200 and T1350 composites tested at 600°C.

Fig. 9. (a) SEM micrograph of the microstructure of T1200 sample and (b) Optical micrograph of the residual imprints on the surface of T1200 after indentation by Berkovich diamond nano-indenter tip.

Fig. 10. Obtained nano-indentation curves (a) load, (b) harmonic contact stiffness, (c) elastic modulus and (d) hardness as a function of contact depth for the existed TiB2, TiB2-corona, TiBw, β-Ti and α-Ti phases in T1200 composite..

Highlights:

- Increased relative density and in-situ formed TiB_W lead to enhanced tensile strength.
- The agglomerated TiB_W and unreacted TiB_2 caused bending strength drop.
- The variation sequence of E and S are: TiB_2 > TiB_2-corona > TiB_W > α -Ti > β-Ti.
- The hardness of TiB_2 was the highest whereas the lowest value found in α-Ti.